Cellular Oncology (2025) 48:675–692
https://doi.org/10.1007/s13402-025-01039-8

RESEARCH

Enhanced ZBTB10 expression induced by betulinic acid inhibits gastric cancer progression by inactivating the ARRDC3/ITGB4/PI3K/AKT pathway

Zhixin Huang[1,2] · Ying Li[3] · Zeyu Zhao[1,2] · Linying Ye[1,2] · Tianhao Zhang[1,2] · Zihan Yu[1,2] · Ertao Zhai[1] · Yan Qian[1] · Xiang Xu[1,2] · Risheng Zhao[1] · Shirong Cai[1] · Jianhui Chen[1,4]

Accepted: 12 January 2025 / Published online: 28 January 2025

Abstract

Background Gastric cancer (GC) ranks as the fourth leading cause of cancer-related deaths worldwide, with most patients diagnosed at advanced stages due to the absence of reliable early detection biomarkers.

Methods RNA-sequencing was conducted to identify the differentially expressed genes between GC tissues and adjacent normal tissues. CCK8, EdU, colony formation, transwell, flow cytometry and xenograft assays were adopted to explore the biological function of ZBTB10 and betulinic acid (BA) in GC progression. RNA-sequencing and phospho-proteomic profiling were performed to analyze the signaling pathways associated with ZBTB10-inhibiting GC progression. Chromatin immunoprecipitation, Co-immunoprecipitation and luciferase reporter assay were employed to elucidate the potential molecular regulatory mechanisms of ZBTB10 in GC.

Results ZBTB10 was one of the most significantly downregulated genes in GC tissues, and higher expression levels of ZBTB10 was correlated with better prognosis in patients with GC. Functional studies revealed that ZBTB10 overexpression and BA inhibited GC progression both in vitro and in vivo. Mechanistically, ZBTB10 enhanced ARRDC3 expression by binding to a specific response element in the ARRDC3 promoter region. Elevated ARRDC3 then directly interacted with β-4 integrin (ITGB4), leading to its ubiquitination and degradation. This cascade ultimately resulted in the downregulation of PI3K and AKT phosphorylation level. Moreover, ZBTB10 was a key target for BA in GC and BA inhibited GC progression through regulating the ZBTB10/ARRDC3/ITGB4/PI3K/AKT axis.

Conclusions Our findings reveal that BA holds promise as an effective therapeutic strategy for GC, and the ZBTB10/ARRDC3/ITGB4/PI3K/AKT axis may serve as a novel diagnostic and therapeutic target.

Keywords Gastric cancer · ZBTB10 · Betulinic acid · ARRDC3 · PI3K/AKT pathway · Malignant progression

Zhixin Huang, Ying Li, Zeyu Zhao and Linying Ye contributed equally to this work.

✉ Shirong Cai
caishr@mail.sysu.edu.cn

✉ Jianhui Chen
chenjh45@mail.sysu.edu.cn

[1] Division of Gastrointestinal Surgery Center, The First Affiliated Hospital of Sun Yat-sen University, Guangzhou, Guangdong 510080, China

[2] Laboratory of Surgery, The First Affiliated Hospital of Sun Yat-sen University, Guangzhou, Guangdong 510080, China

[3] Guangdong Provincial Key Laboratory of Microbial Safety and Health, National Health Commission Science and Technology Innovation Platform for Nutrition and Safety of Microbial Food, State Key Laboratory of Applied Microbiology Southern China, Institute of Microbiology, Guangdong Academy of Sciences, Guangzhou 510070, China

[4] Department of General Surgery, Guangxi Hospital Division of The First Affiliated Hospital, Sun Yat-sen University, Nanning, Guangxi 530000, China

1 Introduction

Gastric cancer (GC) is a prevalent malignancy globally, with around one million new cases diagnosed each year [1, 2]. Despite advancements in treatment, the 5-year survival rate for GC remains below 40%, primarily due to late-stage diagnoses [3, 4]. This underscores the urgent need for reliable early diagnostic and prognostic biomarkers, and a deeper understanding of the molecular mechanism for GC progression.

The transcription factor (TF) zinc finger and BTB domain-containing (ZBTB) 10 belongs to the ZBTB protein family, an emerging family of TFs with critical functions in development, differentiation, and oncogenesis [5, 6]. ZBTB10 has been identified as a downstream target of microRNA-27a and acts as a potential suppressor of the transcription factor Sp1 in various cancers. For instance, Mertens-Talcott et al. found that miR-27a promoted breast cancer progression by regulating the expression of specificity protein TFs, ZBTB10 [7]. Another study revealed that miR-27a regulated the endothelial differentiation of breast cancer stem-like cells through the ZBTB10/VEGF axis [8]. However, recent studies have shown that ZBTB10 also exerted its functions through other mechanisms. Bluhm A et al. found that ZBTB10 could act as a novel variant repeat binding protein at the telomere region of alternative lengthening of telomere [9]. Meanwhile, it has also been found that ZBTB10 transcription factor was crucial for murine cDC1 activation and cytokine secretion [10]. More importantly, androgen-activated ZBTB10 has been confirmed to inhibit prostate cancer progression by negatively regulating PKLR expression [11]. It follows from the above that the potential mechanisms by which ZBTB10 acts are varied. Although direct links between ZBTB10 and GC progression are not yet fully established, genetic variations in hsa-mir-27a that increase miR-27a expression levels and reduce ZBTB10 expression levels were associated with heightened GC risk and metastasis in the Chinese population [12]. This suggests a potential role for ZBTB10 in GC progression and highlights the need for further investigation into its detailed roles and specific mechanisms.

Betulinic acid (BA), derived from the bark of white birch trees, is a pentacyclic triterpenoid with diverse biological activities, including anti-viral, anti-bacterial, anti-oxidant, anti-inflammatory, and anti-fibrotic effects [13–15]. Liu et al. identified BA as a modulator of cannabinoid receptors CB1 and CB2 [16], and it has demonstrated significant anti-tumor activity in cancers such as breast [17], gastric [18], and bladder [19]. The anti-cancer effects of BA were thought to involve various pathways, including the Bmi-1/ROS/AMPK-mTOR-ULK1 pathway in bladder cancer [20] and the NF-κB/VASP pathway in GC [18]. However, there is still a lack of systematic research on the in vivo experiments and underlying mechanisms by which BA inhibits GC progression. Therefore, it is crucial to validate the effect of BA in vivo and explore its mechanisms more systematically.

In this study, we elucidated the inhibiting effects of ZBTB10 and BA in GC progression using both in vitro and in vivo models. We demonstrated that BA-induced upregulation of ZBTB10 transcriptionally activated ARRDC3, which in turn bound to ITGB4, leading to its ubiquitination and degradation. This process ultimately reduced the levels of PI3K and AKT phosphorylation. Our findings suggest that targeting the ZBTB10/ARRDC3/ITGB4/PI3K/AKT axis, alongside BA treatment, could offer promising strategies for GC therapy.

2 Materials and methods

2.1 Patients and tissue specimens

GC tissues and paired adjacent normal tissues were collected from patients diagnosed with GC who underwent surgical resection at the First Affiliated Hospital of Sun Yat-sen University. All tissue specimens were confirmed by pathologic examination and were separated and frozen at -80 °C or formalin-fixed. Written informed consents were obtained from all the patients, and the study was approved by the Ethics Committee of the First Affiliated Hospital of Sun Yat-sen University.

2.2 Cell lines, cell culture, and reagents

Human GC cell lines (AGS, MKN1, MKN28, HGC-27 and MGC803) and normal human gastric epithelial cells-1 (GES-1) were purchased from the Chinese Academy of Sciences, Shanghai Branch Cell Bank. All human cell lines have been authenticated using STR profiling within the last three years, and all experiments were performed with mycoplasma-free cells. AGS cells were cultured in DMEM/F12 (Gibco, Waltham, MA, USA), and MKN1, MKN28, HGC-27, MGC803, and GES-1 cells were cultured in RPMI-1640 (Gibco).

BA (B8936, Sigma Aldrich, St. Louis, MO, USA) was dissolved in DMSO (Sigma Aldrich) as a 20 mM stock solution and stored at -20 °C. LY294002 (HY-10108, MCE, Shanghai, China) was dissolved in DMSO as a 5 mM stock solution and stored at -80 °C. MG-132 (HY-13259, MCE) was dissolved in DMSO as a 10 mM stock solution and stored at -80 °C.

2.3 Construction of stable cell lines and transfection

For the construction of stable overexpression and knockdown GC cell lines, we purchased lentivirus from iGene Biotechnology (Guangzhou, Guangdong, China) and infected GC cells with it. Subsequently, complete media containing 3 μg/mL puromycin (Sigma-Aldrich) were used to screen stably overexpressing and knocked down GC cell lines. Overexpression plasmids were constructed using pEZ-Lv201 (iGene Biotechnology), and knockdown plasmids were constructed using LVRU6GP (iGene Biotechnology). All plasmids and siRNAs were constructed from iGene Biotechnology (Supplementary Table 2). Plasmids and siRNAs transfection were performed using Lipofectamine 3000 (Invitrogen, Carlsbad, CA, USA) according to the manufacturer's instructions.

2.4 Cell viability assay

For the proliferation assays, GC cells (1×10^3/well) were seeded in 96-well plates with six replicates. Proliferation rates were determined using the Cell Counting Kit-8 (CCK-8, Boster Biological Technology, Wuhan, Hubei, China), and measure was performed on a microplate reader (BioTEK, Winooski, VT, USA). For the cell viability assay, 5×10^3 cells per well were inoculated into 96-well plates. After attaching for about 24 h, the culture medium was replaced with complete media containing different concentrations of BA and LY294002 for 24 h. Finally, the absorbance was measured at 450 nm.

2.5 5-Ethynyl-2′-deoxyuridine (EdU) incorporation assay

5×10^3 cells per well were inoculated into 96-well plates. The EdU incorporation assay was conducted using an EdU Staining Kit (RiboBio, Guangzhou, Guangdong, China) according to the manufacturer's instructions. Finally, the cell nucleus was visualized using DAPI, and fluorescence signals were acquired using a fluorescence microscope (Leica, Wetzlar, Germany).

2.6 Colony-forming assays

Cells were seeded separately in 6-well plates at a density of 500/well. The medium was changed twice per week. After 14 days, cells were fixed in 4% paraformaldehyde for 30 min, stained with 0.5% crystal violet for 15 min, rinsed three times with PBS to remove excess dye, photographed, and counted.

2.7 Transwell cell migration and invasion assay

5×10^4 cells resuspended in 400 μL serum-free medium were plated in the upper chamber, while the lower chamber was filled with the complete culture medium. Finally, the cells were fixed with 4% paraformaldehyde and stained with 0.5% crystal violet. Images were acquired using a microscope (Olympus, Tokyo, Japan).

2.8 Cell apoptosis analysis

Cell apoptosis was evaluated by flow cytometric analysis using annexin V-FITC/PI staining (BD Biosciences, San Jose, CA, USA). Apoptotic cells were analyzed using FACSCalibur flow cytometry (BD Biosciences), and FlowJo software (Tree Star Corp, Ashland, WI, USA) was used to analyze the results.

2.9 RNA isolation and quantitative real-time PCR (qRT-PCR)

Total RNA was extracted from tissues and cells using TRIzol reagent (Takara, Beijing, China) according to the manufacturer's protocol. cDNA was generated using the Master Mix cDNA Synthesis Kit (Accurate Biotechnology, Changsha, Hunan, China). qPCR was performed using SYBR Green I (Accurate Biotechnology). The expression levels of the target genes were measured using the $2^{-\Delta\Delta Ct}$ method and normalized to GAPDH as a reference. Each experiment was performed in triplicate and qPCR primers are listed in Supplementary Table 3.

2.10 Protein extracting and western blot (WB)

Western blot was performed as described by Liu [21]. Proteins were extracted from tissues and cells using RIPA lysis buffer (Beyotime, Guangzhou, Guangdong, China) following the manufacturer's protocol and quantified with the bicinchoninic acid protein assay kit (Beyotime). GAPDH was used as a loading control. The antibodies are listed in Supplementary Table 4.

2.11 Phospho-proteomic profiling

ZBTB10-overexpression AGS cells and control cells were washed thrice with PBS and solubilized in lysis buffer. The lysates were resuspended at 4 °C for 30 min by gently pipetting and rocking. Then, the lysates were centrifuged at 14,000 ×*g* for 10 min and transfer the supernatant into a clean test tube. After quantifying the protein concentration with the BCA assay kit (Beyotime), cell lysates containing 400 μg of total protein were firstly diluted and then detected

in Proteome Profiler Human Phospho-Kinase Array (R&D Systems, Minneapolis, MN, USA) according to the manufacturer's instructions.

2.12 Enzyme-linked immunosorbent assay (ELISA)

Concentrations of p-PI3K in AGS and MKN1 cell lysates with ZBTB10 overexpression and knockdown were measured by the ELISA Kits (ml060625, Mlbio, Shanghai, China) according to the manufacturer's instructions.

2.13 Chromatin immunoprecipitation (ChIP)

The ChIP assay was performed using a ChIP assay kit (Cell Signaling Technology, Boston, MA, USA) according to the manufacturer's instructions. Briefly, GC cells were cross-linked with 1% formaldehyde and quenched with glycine (Solarbio, Beijing, China) at room temperature, after which they were collected, washed and resuspended in lysis buffer (Cell Signaling Technology). The digested chromatin was incubated with anti-IgG (DIA-AN, Wuhan, Hubei, China) and anti-ZBTB10 (Abcam) for immunoprecipitation. DNA was purified and analyzed by qRT-PCR.

2.14 Luciferase reporter assay

Plasmid preparation was completed by Genechem (Shanghai, China). AGS and MKN1 cells were transfected with corresponding plasmids using Lipofectamine 3000 (Invitrogen). After 48 h, 20 μM BA was added to the medium and treated for 24 h. Luciferase activity was detected by the Multifunctional enzyme marker (Thermo).

2.15 Co-immunoprecipitation (Co-IP)

The cells were collected and were lysed on ice with IP lysate. Lysates were centrifuged for 10 min (12,000 ×*g*, 4 °C), and the supernatant was collected. Subsequently, the supernatant was incubated with corresponding primary antibodies overnight at 4 °C. The next day, protein A/G Magnetic Beads were added to the samples and incubated for 4 h at 4 °C. The beads were washed five times and then denatured at 97 °C for 7 min prior to WB analysis.

2.16 MG-132 treatment

For the ubiquitination assay, the GC cells were pretreated with the indicated plasmids for 48 h. After treated with 20 μM MG-132 for 6 h, the cells were lysed by IP lysis buffer. Next, immunoprecipitation against the corresponding protein was performed. Finally, the immunoprecipitants were subjected to WB.

2.17 Cellular immunofluorescence (IF)

AGS cells with stable ARRDC3 overexpression and negative control were seeded onto the chamber slides. After attaching for about 24 h, the cells on chamber slides were washed with PBS and fixed in 4% paraformaldehyde for 15 min at room temperature, followed by exposure to 0.3% Triton X-100 for 20 min. Subsequently, the cells were blocked in 2% goat serum for 1 h and incubated with specific primary antibodies overnight at 4 °C. The next day, cells were incubated fluorescent secondary antibodies corresponding to the species in dark for 2 h and DAPI was used for nuclear staining. Finally, images were acquired using a confocal microscope (FV3000, Olympus).

2.18 Immunohistochemistry (IHC)

The tissues were fixed with 10% paraformaldehyde and embedded in paraffin. After deparaffinization, rehydration, and antigen retrieval, the samples were incubated with primary antibodies using the corresponding antibodies. Images were taken with an Axio Scope.A1 398 vertical microscope (Leica). The final immunoreactive score (IRS) was obtained by multiplication of the intensity score and the quantity score. Briefly, two investigators independently scored the percentage of positive-stained cells (%PC) from 0 to 4 (0: no positive cells; 1: <10%; 2: 10–50%; 3: 51–80%; 4: >80%) and the staining intensity from 0 to 3 (0: no staining; 1: weak staining; 2: moderate staining; 3: strong staining). The IRS was then calculated as the product of these two scores (range, 0–12). We defined an IRS score of less than 6 as low expression and the rest as high expression.

2.19 Animal studies

Female BALB/c nude mice (5 weeks old) were obtained from Specific Pathogen-Free Biotechnology Co., Ltd. (Beijing, China) and housed under specific pathogen-free conditions. All animal experiments were performed with the approval of the Animal Care and Use Committee of the Sun Yat-sen University.

For the xenograft model, MGC803 cells (5×10^6 in 100 μL PBS) with ZBTB10 overexpression and negative control were subcutaneously injected into each flank of nude mice (six mice/group). Tumor size was measured every 3 days (volume = length × width^2 × 1/2). The mice were sacrificed 21 days after tumor cell implantation. The tumors were weighed, imaged, fixed in 4% paraformaldehyde. To investigate the function of BA, xenograft models were established using MGC803 cells with knockdown ZBTB10 and negative control according to the methods in previous studies [17]. Seven days later, the tumors grew to approximately

100 mm^3, and tumor-bearing mice were randomly assigned to four groups.

For the lung metastasis model, MGC803 cells (1×10^6 in 100 μL PBS) overexpressing ZBTB10 and the negative control were injected into the tail vein of nude mice. The mice were sacrificed 8 weeks after GC cell injection and pulmonary metastatic nodules were counted. Finally, the lungs were resected, photographed, and fixed in 4% paraformaldehyde for further analyses. Similarly, we explored the effect of BA on lung metastasis according to a previous study [22].

For the popliteal lymph node metastasis model, MGC803 cells (1×10^6 in 20 μL PBS) with ZBTB10 overexpression and negative control were injected into the left footpad of mice (twice in 3 days). The mice were sacrificed after 8 weeks, and the lymph node transfer ratio was determined. The footpad and popliteal lymph nodes of the left leg were resected, photographed, and fixed in 4% paraformaldehyde for further analyses.

2.20 Statistical analysis

All statistical analyses were performed using SPSS 22.0 (IBM, Chicago, IL, USA) and GraphPad Prism 8.0 (GraphPad, La Jolla, CA, USA). All results were presented as the mean ± standard deviation (SD) of data from independent bio-triplications. Data analysis in each group was performed using Student's t-test, and one-way or two-way analysis of variance. Kaplan-Meier analysis was used to determine the survival differences. $P < 0.05$ was considered to indicate a statistically significant difference.

3 Results

3.1 ZBTB10 is significantly downregulated in GC and correlated with positive prognosis

To identify genes closely associated with the development and progression of GC, we conducted RNA-sequencing on five pairs of GC tissues and adjacent normal tissues. Our analysis revealed 442 differentially expressed genes ($p < 0.01$, $\log_2 FC > 2.0$), including 280 upregulated and 162 downregulated genes in GC tissues (Fig. 1A, and Supplementary Table 6). While ZBTB protein family has been implicated in various tumors, their research in GC is limited. Notably, our transcriptome data identified ZBTB10 as one of the most significantly downregulated genes in GC (Fig. 1A). Therefore, ZBTB10 was chosen for further exploration. To validate these findings, we examined ZBTB10 mRNA expression in 59 GC cases using qRT-PCR. The results showed a marked downregulation of ZBTB10 mRNA levels in GC tissues compared to adjacent normal tissues ($n = 59$, $p = 0.00073$; Fig. 1B). Moreover, consistent with the mRNA levels, ZBTB10 protein levels were also significantly downregulated in GC tissues (Fig. 1C, D, and Supplementary Fig. 1A). Additionally, we also quantified ZBTB10 expression levels in GES-1 and common GC cell lines. The results showed that ZBTB10 expression levels were lower in GC cells compared to that in GES-1 (Fig. 1E, F). Overall, all of the above results indicate that ZBTB10 is lowly expressed in GC.

Next, to elucidate the clinical prognostic relevance of ZBTB10 in GC, we performed IHC staining on a tissue microarray containing samples from 94 GC patients. We categorized ZBTB10 expression into high and low expression groups based on IRS (Fig. 1G). Analysis of clinicopathologic parameters revealed that lower ZBTB10 expression was associated with worse T stage and more advanced tumor stage (Supplementary Table 1). Furthermore, Kaplan–Meier survival analysis showed that lower ZBTB10 expression in GC tissues contributed to poorer prognosis ($n = 94$, $p < 0.001$; Fig. 1H). More importantly, multifactorial Cox regression analysis confirmed ZBTB10 as an independent prognostic predictor (Fig. 1I), suggesting its potential as a valuable diagnostic biomarker for GC. Taken together, these findings indicate that ZBTB10 is significantly downregulated in GC and that lower ZBTB10 expression is correlated with worse prognosis.

3.2 ZBTB10 inhibits GC cells proliferation, metastasis, and anti-apoptotic capabilities in vitro

We next attempted to clarify the role of ZBTB10 in GC progression. Firstly, we constructed AGS, MKN1, HGC-27, and MGC803 cells with stable ZBTB10 overexpression and knockdown, and the efficiencies of stable ZBTB10 overexpression and knockdown were verified by qRT-PCR and WB (Fig. 2A, B, and Supplementary Fig. 1D, 2A). Then, gain or loss-of-function experiments were conducted. The CCK-8, EdU, and colony formation assays demonstrated that ZBTB10 overexpression significantly inhibited GC cell growth within 4 days and reduced the percentage of EdU cells and the number of colonies, and vice versa (Fig. 2C–H, and Supplementary Fig. 1B, 1E–G, 2B, 2C). Next, to examine the effect of ZBTB10 on the metastatic capabilities of GC cells, we performed transwell migration and matrigel invasion assays. The results indicated that ZBTB10 knockdown significantly increased the migration and invasion capabilities of GC cells, whereas ZBTB10 overexpression inhibited these processes (Fig. 2I, J, and Supplementary Fig. 1C, 1H, 2D). Meanwhile, apoptosis assays also revealed that the proportion of apoptotic cells was significantly reduced upon ZBTB10 knockdown, whereas the proportion

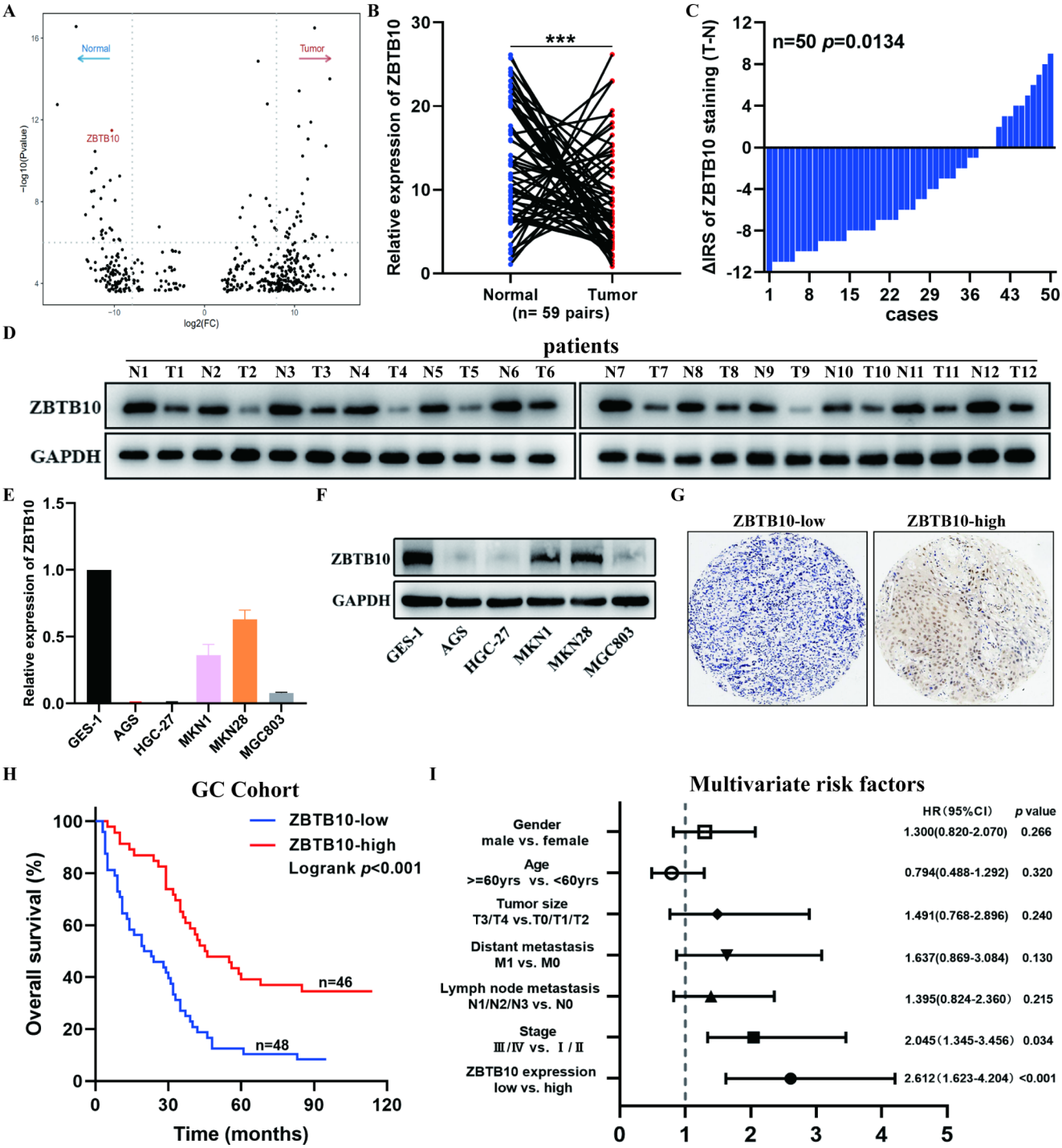

Fig. 1 ZBTB10 is significantly downregulated in GC and correlated with positive prognosis. **A** Volcano plot showed the differential expression genes between five pairs of GC tissues and their paired adjacent normal tissues. x axis demonstrated the fold changes of read density and y axis showed the adjusted *p* value. **B** Relative expression levels of ZBTB10 in GC tissues and their paired adjacent normal tissues were detected by qRT-PCR ($n=59$, $p=0.00073$). **C** Differential distribution of ZBTB10 immunoreactivity score (IRS) (ΔIRS = IRST-IRSN) ($n=50$, $p=0.0134$). **D** ZBTB10 protein levels in GC tissues and their paired adjacent normal tissues were detected by western blotting ($n=12$). **E**, **F** The mRNA (E) and protein (F) expression levels of ZBTB10 in GES-1 and different GC cell lines. **G** Representative images of IHC staining for ZBTB10-low and ZBTB10-high in tissue microarray. **H** Kaplan–Meier survival analysis revealed that low expression of ZBTB10 was correlated with shorter overall survival time in GC patients ($n=94$, $p<0.001$, log-rank test). **I** Multivariate analysis showed that ZBTB10 expression level was one of independent risk factor in our GC cohort. Data are expressed as mean ± SD of biological replicate experiments. *$p<0.05$, **$p<0.01$, ***$p<0.001$

of apoptotic cells was increased upon ZBTB10 overexpression (Fig. 2K–L, and Supplementary Fig. 1I, 2E). The above results suggest that ZBTB10 could inhibit GC cells proliferation, metastasis, and anti-apoptotic capabilities in vitro.

3.3 ZBTB10 overexpression inhibits the growth and metastasis of GC in vivo

To confirm our in vitro findings and explore the biological role of ZBTB10 in vivo, we constructed a BALB/c nude mouse model using MGC803 cells with stable ZBTB10 overexpression and negative control cells. In the subcutaneous xenograft model, compared with tumors from negative control cells, tumors derived from ZBTB10-overexpressing cells exhibited significantly reduced growth, both in terms of volume and weight (Fig. 3A–C, and Supplementary Fig. 3A). IHC analysis further revealed increased ZBTB10 expression and a higher proportion of apoptotic cells in the ZBTB10-overexpression group, alongside reduced Ki-67 expression (Fig. 3D). Furthermore, we also explored whether ZBTB10 could affect the metastasis of GC in vivo by constructing a lung metastasis model and a footpad-popliteal lymph node (LN) metastasis model. As expected, ZBTB10 overexpression significantly inhibited lung metastasis, with fewer metastatic nodules observed in the ZBTB10-overexpression group compared to the negative control (Fig. 3E–G, and Supplementary Fig. 3B, C). In the footpad-popliteal LN metastasis model, LNs from mice injected with ZBTB10-overexpressing cells were smaller than those from the negative control cells (Fig. 3H–J, and Supplementary Fig. 3D). Moreover, HE staining revealed that LNs of the ZBTB10 overexpression group had a lower percentage of metastasis compared with the negative control group (Fig. 3K, L). Collectively, these observations demonstrate that ZBTB10 also plays a crucial role in inhibiting GC growth and metastasis in vivo.

3.4 ZBTB10 exerts biological functions through inactivating the PI3K/AKT pathway

To pursue the underlying molecular mechanism of ZBTB10 inhibiting GC progression, we conducted whole genome RNA-sequencing and subsequent functional enrichment analysis between AGS cells with the negative control and ZBTB10 overexpression. Our sequencing data revealed that ZBTB10 overexpression resulted in altered expression of 323 genes (Supplementary Fig. 4A, and Supplementary Table 7). Further pathway analysis of these differentially expressed genes showed that ZBTB10 overexpression inhibited the activation of multiple cancer-promoting pathways, such as the PI3K/AKT pathway, the MAPK pathway, and the Ras pathway (Supplementary Fig. 4B). Among them, the PI3K/AKT pathway was the most affected pathway by ZBTB10 overexpression (Supplementary Fig. 4B). To further investigate this relationship, we performed a Phosphoproteomic profiling to detect changes in the expression levels of common phosphorylated proteins upon ZBTB10 overexpression. The results showed that phosphorylation of AKT was significantly inhibited after ZBTB10 overexpression (Fig. 4A). Furthermore, ELISA and WB also demonstrated that ZBTB10 overexpression reduced the protein levels of p-PI3K and p-AKT in AGS and MKN1 cells, whereas ZBTB10 knockdown had the opposite effect (Fig. 4B, C). Consequently, we propose the hypothesis that ZBTB10 inhibits GC progression through inactivating the PI3K/AKT pathway.

Subsequently, we constructed in vitro functional rescue experiments. We used the PI3K inhibitor LY294002 (LY2; 10 μM) [23] to block the PI3K/AKT pathway in ZBTB10-knockdowning cells and detected the proteins levels by WB (Fig. 4D, F). Inactivation of the PI3K/AKT pathway reversed the promoting effect on GC cells induced by ZBTB10 knockdown (Fig. 4E, G, and Supplementary Fig. 4D–F). Similarly, targeting AKT with siRNAs in ZBTB10-knockdown cells yielded results consistent with PI3K inhibition (Fig. 4H-K, and Supplementary Fig. 4G–I). Through these data, we summarize that ZBTB10 inhibits the proliferation, metastasis, and anti-apoptotic capabilities of GC cells through inactivating the PI3K/AKT pathway.

3.5 Enhanced ARRDC3 expression induced by ZBTB10 inhibits the PI3K/AKT pathway by promoting the ubiquitination and degradation of ITGB4

We then explored the detailed mechanism of ZBTB10 inactivating the PI3K/AKT pathway. Through further comprehensive analysis of sequencing data, we found that ZBTB10 overexpression promoted ARRDC3 expression (Supplementary Fig. 5A). Furthermore, Chip-sequencing data from GEO (GSE105183) and the Genecards database (https://www.genecards.org/) both revealed that there were the direct interaction sites between ZBTB10 and the ARRDC3 promoter region. Notably, previous studies have shown that ARRDC3 inhibited liver fibrosis and epithelial-to-mesenchymal transition via the ITGB4/PI3K/AKT pathway [24]. Thus, we hypothesized that ZBTB10 might promote ARRDC3 expression through transcriptional activation, thereby inhibiting the PI3K/AKT pathway and GC progression. To confirm our hypothesis, we quantified ARRDC3 mRNA and protein levels in cells with ZBTB10 overexpression and knockdown using qRT-PCR and WB. The results indicated that ZBTB10 overexpression led to elevated ARRDC3 levels, while ZBTB10 knockdown

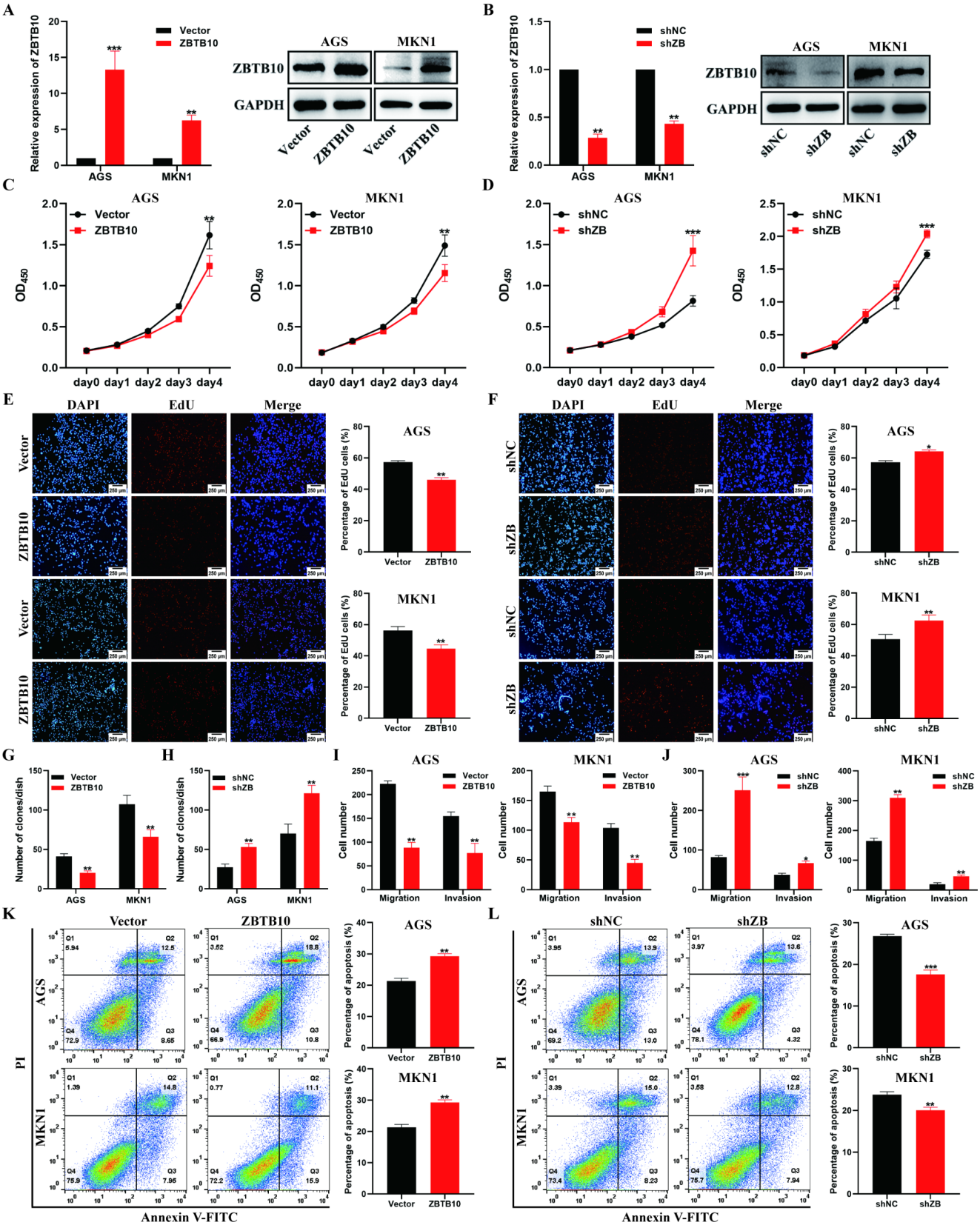
A
Relative expression of ZBTB10
Vector
ZBTB10
AGS
MKN1
ZBTB10
GAPDH
B
shNC
shZB
C
OD450
day0 day1 day2 day3 day4
D
E
DAPI
EdU
Merge
Percentage of EdU cells (%)
F
G
Number of clones/dish
H
I
Cell number
Migration
Invasion
J
K
PI
Annexin V-FITC
Percentage of apoptosis (%)
L

Fig. 2 ZBTB10 inhibits GC cells proliferation, metastasis, and anti-apoptotic capabilities in vitro. **A**, **B** The stably overexpression (A) and knockdown (B) efficiencies of ZBTB10 were measured by qRT-PCR and western blotting in AGS and MKN1 cells. **C**, **D** ZBTB10 overexpression suppressed the proliferation of AGS and MKN1 cells (C) while ZBTB10 knockdown promoted (D) as assessed by CCK-8 assay. **E**, **F** Representative images of EdU assay in transfected GC cells (left panel) and quantitative results (right panel), DAPI (blue), EdU (red). **G**, **H** Quantitative results of colony formation assay in transfected GC cells. **I**, **J** Quantitative results of transwell assay in transfected GC cells. **K**, **L** Representative images of flow cytometric cell apoptosis analysis in transfected GC cells (left panel) and quantitative results (right panel). Data are expressed as mean ± SD of biological replicate experiments. *$p<0.05$, **$p<0.01$, ***$p<0.001$

reduced them (Fig. 5A, B). Moreover, IHC staining of the previous subcutaneous tumor samples also showed that ZBTB10 overexpression upregulated ARRDC3 expression (Fig. 5C). We then assessed ARRDC3 expression in GC tissues and cell lines; the results revealed that ARRDC3 was downregulated in GC tissues and cell lines, and there was a significantly positive correlation between ZBTB10 and ARRDC3 expression in GC tissues (Fig. 5D, E, and Supplementary Fig. 5B). Meanwhile, lower ARRDC3 expression was associated with shorter overall survival in patients with GC (Fig. 5F, and Supplementary Fig. 5C). Gain- and loss-of-function studies further demonstrated that ARRDC3 overexpression inhibited GC cell proliferation and metastasis while promoting apoptosis, whereas ARRDC3 knockdown had the opposite effects (Supplementary Fig. 5D–I). To verify that ZBTB10 promoted ARRDC3 expression through a transcription mechanism, we conducted ChIP and dual-luciferase reporter assays. ZBTB10 overexpression enhanced the binding ability of ZBTB10 to the promoter region of ARRDC3 (Fig. 5G), whereas ZBTB10 knockdown reduced it (Fig. 5H). Correspondingly, ZBTB10 overexpression increased reporter activity (Fig. 5I), whereas ZBTB10 knockdown decreased it (Fig. 5J), supporting the hypothesis of ZBTB10-mediated transcriptional activation of ARRDC3. Finally, we performed rescue experiments by knocking down ARRDC3 in LCN2-overexpressing AGS cells and overexpressing ARRDC3 in ZBTB10-knockdown MKN1 cells. Results showed that ARRDC3 knockdown rescued the proliferation, migration, and invasion abilities of ZBTB10-overexpressing AGS cells (Fig. 5K, and Supplementary Fig. 5J, K), and ARRDC3 overexpression eliminated the promoting effect of ZBTB10 knockdown in GC progression (Fig. 5L, and Supplementary Fig. 5L, M). These results suggest that ZBTB10 functions as a TF to upregulate ARRDC3, which is a potential tumor suppressor gene and a key downstream target in ZBTB10-regulated GC progression.

As previously demonstrated, ARRDC3 inhibited tumor progression by negatively regulating ITGB4 [25, 26], and the integrin family was known to be one of the regulators of the PI3K/AKT pathway [27]. To explore whether ARRDC3 demonstrates the above mechanism in GC, we examined the expression of ITGB4, p-PI3K, and p-AKT following ARRDC3 overexpression and knockdown. WB analyses showed that ARRDC3 overexpression markedly reduced ITGB4, p-PI3K, and p-AKT levels, whereas ARRDC3 knockdown had the opposite effect (Fig. 5M). Moreover, IF analysis showed that ITGB4 surface levels were significantly down-regulated in cells with ARRDC3 overexpression (Fig. 5N). It has been reported that ARRDC3 promoted protein degradation by mediating ubiquitination levels [25, 28]. Therefore, we next sought to elucidate whether ARRDC3 inhibits ITGB4 expression by promoting its ubiquitination level. We found that treatment with the proteasome inhibitor MG-132 (20 μM) prevented the ARRDC3-mediated decrease in ITGB4 levels (Fig. 5O). Furthermore, Co-IP assays also indicated that MG-132 could reverse the ubiquitination of ITGB4 induced by ARRDC3 (Fig. 5P). More importantly, we found that ARRDC3 overexpression could counteract the elevation in ITGB4, p-PI3K, and p-AKT levels induced by ZBTB10 knockdown, indicating that ARRDC3 was indispensable for the ZBTB10-mediated inhibition of the ITGB4/PI3K/AKT pathway (Fig. 5Q). Collectively, these results demonstrate that ZBTB10 transcriptionally activates ARRDC3 and then enhanced ARRDC3 directly binds to ITGB4 leading to its ubiquitination and degradation, which in turn downregulates PI3K and AKT phosphorylation.

3.6 ZBTB10 is a pivotal target for BA in inhibiting GC progression

Emerging evidences have suggested that ZBTB10 might be a target of multiple anti-cancer drugs [29, 30], but this has not been reported in GC. To explore whether ZBTB10 is the target for a drug with anti-GC effects, we made predictions using the connectivity map (CMap) database [31] combined with the sequencing data of control cells and ZBTB10-overexpressing cells (Fig. 6A). The results showed that the differentially expressed genes after ZBTB10 overexpression were basically consistent with those affected by BA treatment (Supplementary Table 5). Additionally, ZBTB10 has been reported as a target of BA in breast and colon cancers. Therefore, we hypothesized that ZBTB10 might also be a target of BA in GC. Firstly, we performed cell viability assays and found that BA inhibited GC cell proliferation in a concentration- and time-dependent manner, with IC-50 values of 40.46 μM and 40.17 μM for AGS and MKN1 cells, respectively, after 24 h of treatment (Supplementary Fig. 6A, B). Subsequently, treatment of AGS and MKN1 cells with 20 μM BA [18] for 24 h confirmed that BA increased ZBTB10 mRNA and protein levels, while

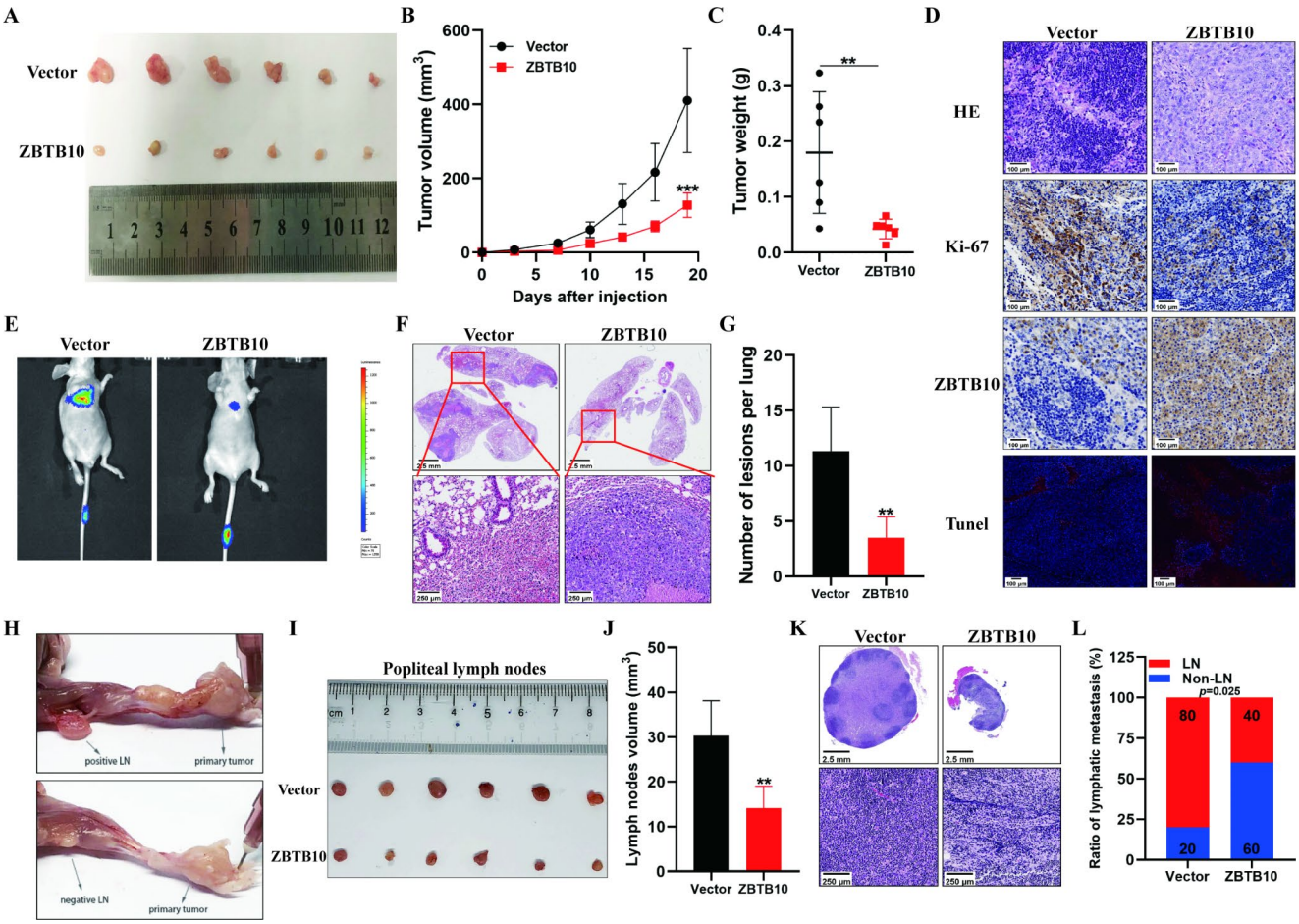

Fig. 3 ZBTB10 overexpression inhibits the growth and metastasis of GC in vivo. **A**–**C** Images of xenograft tumor samples (A), tumor volumes (B), and tumor weights (C) derived from ZBTB10 overexpressing and negative control MGC803 cells, scale bar:200 μm. **D** Representative images of HE staining and IHC staining for ZBTB10, Ki-67 and Tunel ($n=6$). **E** Representative bioluminescence images of mice, 8 weeks after tail vein injection of negative control and ZBTB10 overexpression MGC803 cells. **F** Representative HE staining images of lung samples from mice with the injection of MGC803 cells with negative control and ZBTB10 overexpression. Scale bars:2.5 mm (upper panel) and 250 μm (bottom panel). **G** Quantitative results of the metastatic nodes of the lungs in Fig. 3F. **H** Representative images of popliteal lymph node metastasis and non-metastatic mice eight weeks after footpad injection with the indicated cells. **I** Images of the popliteal lymph nodes of mice injected with the indicated cells. **(J)** The volume of popliteal lymph nodes in Fig. 3I. **K** Representative HE staining images of popliteal lymph nodes in Fig. 3I. Scale bars:2.5 mm (upper panel) and 250 μm (lower panel). **L** Percentage of metastatic and non-metastatic popliteal lymph nodes in the indicated groups. Data are expressed as mean ± SD of biological replicate experiments. *$p<0.05$, **$p<0.01$, ***$p<0.001$

decreasing p-PI3K and p-AKT levels in a concentration-dependent manner (Fig. 6B, C). The above results indicate that ZBTB10 may be a potential target of BA in GC, and that BA may inhibit GC progression through the ZBTB10/PI3K/AKT pathway.

To further validate this, we conducted rescue experiments with DMSO and 20 μM BA in control and ZBTB10 knockdown cells. BA treatment decreased the upregulation of p-PI3K and p-AKT induced by ZBTB10 knockdown (Fig. 6D, I), and ZBTB10- and ARRDC3-knockdown GC cells exhibited increased resistance to BA (Fig. 6E, J, and Supplementary Fig. 6C, D). Moreover, ZBTB10 knockdown partially rescued the inhibition of colony formation, metastasis, and anti-apoptotic effects induced by BA treatment in GC (Fig. 6F–H, K–M, and Supplementary Fig. 6E, F). Collectively, these findings confirm that ZBTB10 is a target of BA in GC, and that BA inhibits GC progression via the ZBTB10/ARRDC3/ITGB4/PI3K/AKT pathway.

3.7 BA inhibits GC tumorigenicity and metastasis by promoting ZBTB10 expression in vivo

Finally, we assessed whether BA could inhibit GC progression in vivo and whether this effect depends on ZBTB10. We constructed a rescue mouse model with MGC803-shNC and MGC803-shZBTB10 cells, treated with or without BA. In the subcutaneous xenograft model, BA treatment delayed tumor growth in terms of both volume and weight,

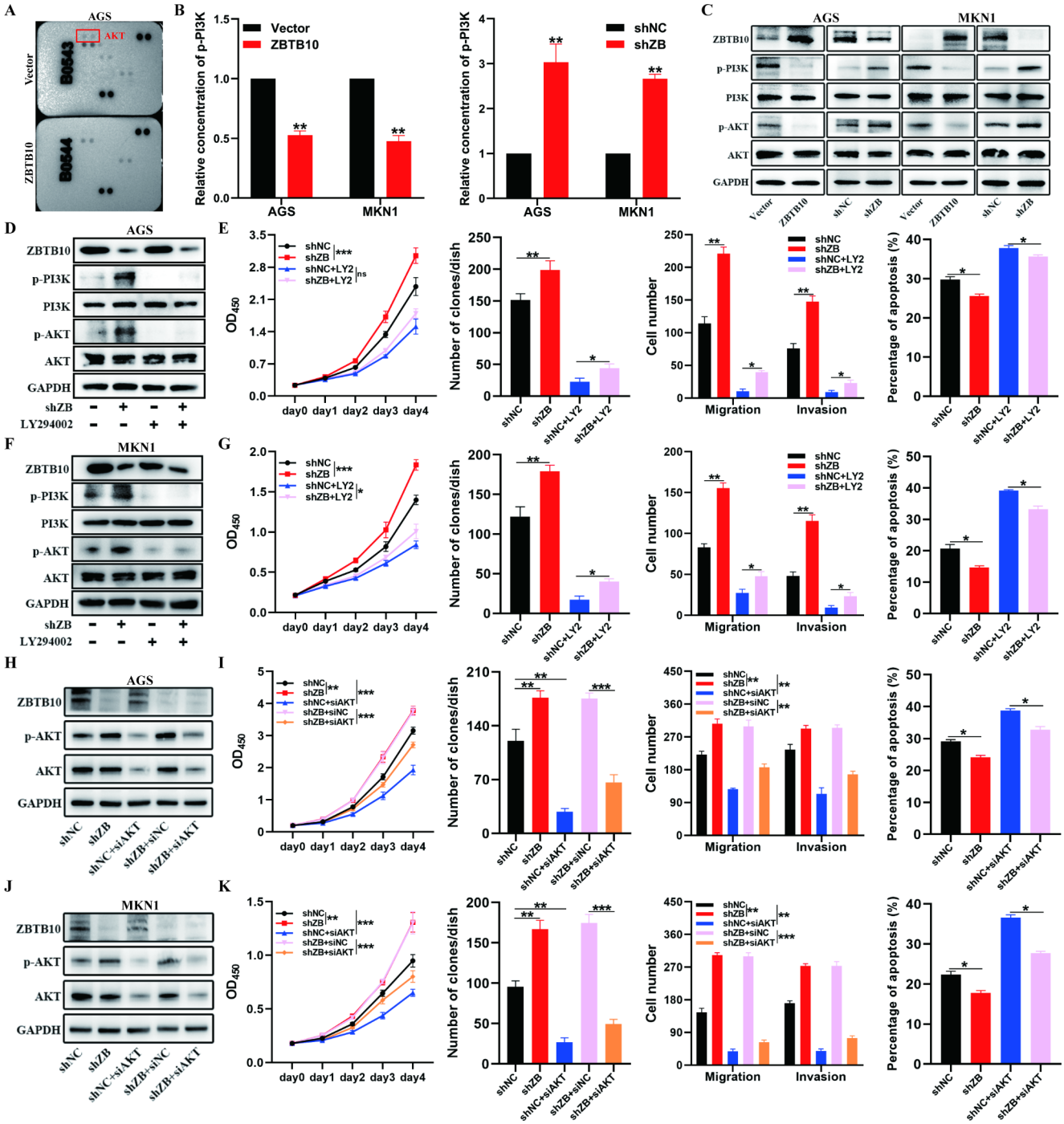

Fig. 4 ZBTB10 exerts biological functions through inactivating the PI3K/AKT pathway. **A** The result of Phospho-proteomic profiling showed ZBTB10 overexpression inhibited the expression of p-AKT. **B** The concentrations of p-PI3K with ZBTB10 overexpression and knockdown were detected by ELISA. **C** The protein levels of PI3K, AKT, p-PI3K and p-AKT in AGS and MKN1 cells with ZBTB10 overexpression and knockdown were detected by western blotting. **D**, **F** p-PI3K and p-AKT protein levels were increased following ZBTB10 knockdown and were rescued by LY294002 (the PI3K inhibitor, 10μM) treatment. **E**, **G** The malignant biological behavior of AGS (E) and MKN1 (G) cells was enhanced when ZBTB10 knockdown, and this effect was rescued after LY294002 treatment. **H**, **J** p-AKT protein level was increased following ZBTB10 knockdown and was rescued by AKT siRNAs. **I**, **K** CCK-8, colony formation assay, transwell assay and flow cytometric cell apoptosis analysis revealed that AKT knockdown rescued the enhancement of malignant biological behavior caused by ZBTB10 knockdown in AGS (I) and MKN1 (K) cells. Data are expressed as mean ± SD of biological replicate experiments. $*p<0.05$, $**p<0.01$, $***p<0.001$

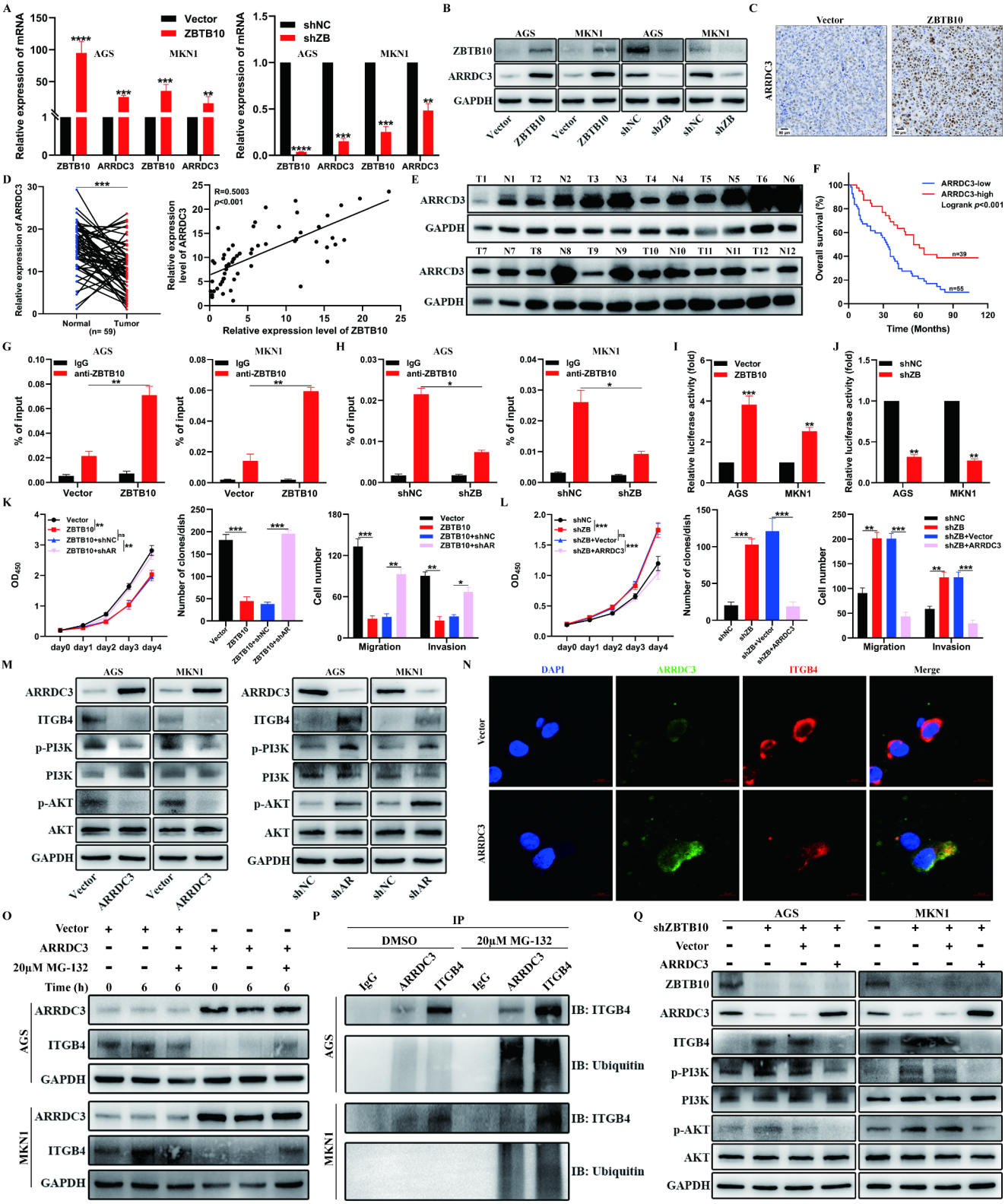
A
Relative expression of mRNA
Vector
ZBTB10
shNC
shZB
AGS
MKN1
ZBTB10
ARRDC3
B
ZBTB10
ARRDC3
GAPDH
Vector
shNC
shZB
C
Vector
ZBTB10
ARRDC3
D
Relative expression of ARRDC3
Normal
Tumor
(n= 59)
R=0.5003
p<0.001
Relative expression level of ARRDC3
Relative expression level of ZBTB10
E
T1 N1 T2 N2 T3 N3 T4 N4 T5 N5 T6 N6
T7 N7 T8 N8 T9 N9 T10 N10 T11 N11 T12 N12
F
ARRDC3-low
ARRDC3-high
Logrank p<0.001
Overall survival (%)
Time (Months)
n=39
n=55
G
IgG
anti-ZBTB10
% of input
H
I
Relative luciferase activity (fold)
J
K
Vector
ZBTB10
ZBTB10+shNC
ZBTB10+shAR
OD450
day0 day1 day2 day3 day4
Number of clones/dish
Cell number
Migration
Invasion
L
shNC
shZB
shZB+Vector
shZB+ARRDC3
M
ARRDC3
ITGB4
p-PI3K
PI3K
p-AKT
AKT
GAPDH
N
DAPI
ARRDC3
ITGB4
Merge
O
20μM MG-132
Time (h)
P
IP
DMSO
IB: ITGB4
IB: Ubiquitin
Q
shZBTB10

Fig. 5 Enhanced ARRDC3 expression induced by ZBTB10 inhibits the PI3K/AKT pathway by promoting the ubiquitination and degradation of ITGB4. **A**, **B** The ARRDC3 mRNA (A) and protein (B) expression levels in GC cells with ZBTB10 overexpression or knockdown. **C** Representative images of IHC staining for ARRDC3 expression of xenograft tumor tissues. Scale bar: 50 μm. **D** Relative expression levels of ARRDC3 in GC tissues and their paired adjacent normal tissues were detected by qRT-PCR ($n=59$, $p=0.00083$), and the mRNA expression levels of ARRDC3 in GC tissues were positively correlated with the mRNA expression level of ZBTB10. **E** ARRDC3 protein levels in GC tissues and their paired adjacent normal tissues were detected by western blotting ($n=12$). **F** Kaplan–Meier survival analysis revealed that low expression of ARRDC3 was correlated with shorter overall survival time in GC patients ($n=94$, $p<0.001$; log-rank test). **G** ChIP-qPCR analysis demonstrated that overexpression of ZBTB10 enhanced the binding of ZBTB10 and ARRDC3 promoter region. **H** ChIP-qPCR analysis demonstrated that knockdown of ZBTB10 weakened the binding of ZBTB10 and ARRDC3 promoter region. **I** Relative luciferase activity of ARRDC3 in AGS and MKN1 cells with negative control and ZBTB10 overexpression. **J** Relative luciferase activity of ARRDC3 in AGS and MKN1 cells with negative control and ZBTB10 knockdown. **K** CCK-8, colony formation assay, and transwell assay revealed that ARRDC3 knockdown rescued the suppression of proliferation and metastasis abilities caused by ZBTB10 overexpression. **L** CCK-8, colony formation assay, and transwell assay showed that the proliferation and metastasis abilities increased upon ZBTB10 knockdown, and this effect was inhibited by ARRDC3 overexpression. **M** The protein levels of ITGB4, PI3K, AKT, p-PI3K and p-AKT in AGS and MKN1 cells with ARRDC3 overexpression and knockdown were detected by western blotting. **N** Immunofluorescence shows that ARRDC3 and ITGB4 have the same subcellular localization, and ARRDC3 overexpression inhibits ITGB4 expression. **O** ARRDC3 overexpression reduced ITGB4 expression, and MG-132 stimulation increased ITGB4 expression. **P** ARRDC3 regulates ITGB4 expression through the ubiquitin-proteasome pathway. **Q** ZBTB10-knockdown GC cells were transfected with the plasmid of negative control and ARRDC3 for 48 h, and then subjected to western blotting assays. Data are expressed as mean ± SD of biological replicate experiments. *$p<0.05$, **$p<0.01$, ***$p<0.001$

and ZBTB10 knockdown partially reversed this effect (Fig. 7A–C, and Supplementary Fig. 7A). Correspondingly, Ki-67 expression decreased, and ZBTB10 expression and apoptosis rates increased with BA treatment (Fig. 7G). Most importantly, BA did not cause significant weight loss and induce any morphological variations nor functional changes in the liver, heart, spleen, lung, and kidney throughout the experiment (Fig. 7D–F). Similarly, in the lung metastasis model, BA significantly inhibited lung metastasis, and ZBTB10 knockdown diminished this effect (Fig. 7H, I, and Supplementary Fig. 7B). These results confirm that BA inhibits GC tumorigenicity and metastasis by promoting ZBTB10 expression in vivo.

4 Discussion

Most patients with GC are diagnosed at advanced stages, which significantly complicates treatment options [32]. Despite numerous efforts to explore for the early diagnostic methods, reliable molecular biomarkers for GC remain largely unidentified. The ZBTB protein family, characterized by their zinc finger domains, encompasses a group of TFs involved in various biological processes, including gene regulation, DNA recognition, RNA packaging, apoptosis regulation, and protein folding and assembly [33, 34]. Moreover, these proteins can act as either tumor promoters or suppressors depending on the context [35]. In our study, RNA-sequencing identified ZBTB10 as one of the most downregulated genes in GC. ZBTB10 is a novel member of the ZBTB transcription factors, and its biological role has not been fully elucidated. Previous studies have reported that ZBTB10 functions as a transcriptional inhibitor of SP1 and plays a role in inhibiting tumor activities, suggesting that ZBTB10 should be considered a tumor suppressor [36]. Notably, in a pivotal investigation examining the nexus between mutations in miRNA and susceptibility of GC, reduced ZBTB10 mRNA level was found to be associated with the increased risk and metastasis of GC [12], suggesting that ZBTB10 may inhibit GC progression. Our findings confirmed that ZBTB10 was significantly downregulated in GC tissues compared to normal tissues. Further analysis revealed that down-regulated ZBTB10 expression in patients with GC was an independent risk factor and closely correlated with lower survival rate. Similarly, we also draw the same conclusion in cell function and animal experiments. To the best of our knowledge, this is the first study to determine the role of ZBTB10 in GC progression.

The PI3K/AKT pathway is one of the major cellular signaling pathways that plays an important role in basic intracellular functions [37]. It is crucial for regulating cell growth, survival, and metabolism, and its dysregulation is implicated in numerous human cancers [38]. Furthermore, researches have also confirmed the involvement of PI3K/AKT pathway in GC progression and the association with poor outcomes [39, 40]. Our study was the first to demonstrate that ZBTB10 inhibited the PI3K/AKT pathway activation. More importantly, inactivating the PI3K/AKT pathway via LY294002 and siRNAs targeting AKT was proved to effectively counteract the malignant behaviors regulated by ZBTB10, which validated ZBTB10-hindering GC progression through the PI3K/AKT pathway inactivation.

However, the detailed mechanism of ZBTB10-mediated the PI3K/AKT pathway inactivation in GC remains unclear. Through comprehensive analysis of sequencing data, we identified ARRDC3 as one of the pivotal targets of ZBTB10. ARRDC3, a member of the arrestin superfamily, is known to inhibit tumor progression by negatively regulating ITGB4, a protein linked to aggressive tumor behavior [25, 41]. For instance, it has been reported that ARRDC3 inhibited breast cancer progression by negatively regulating ITGB4 [25]. Another study showed that ARRDC3 inhibited

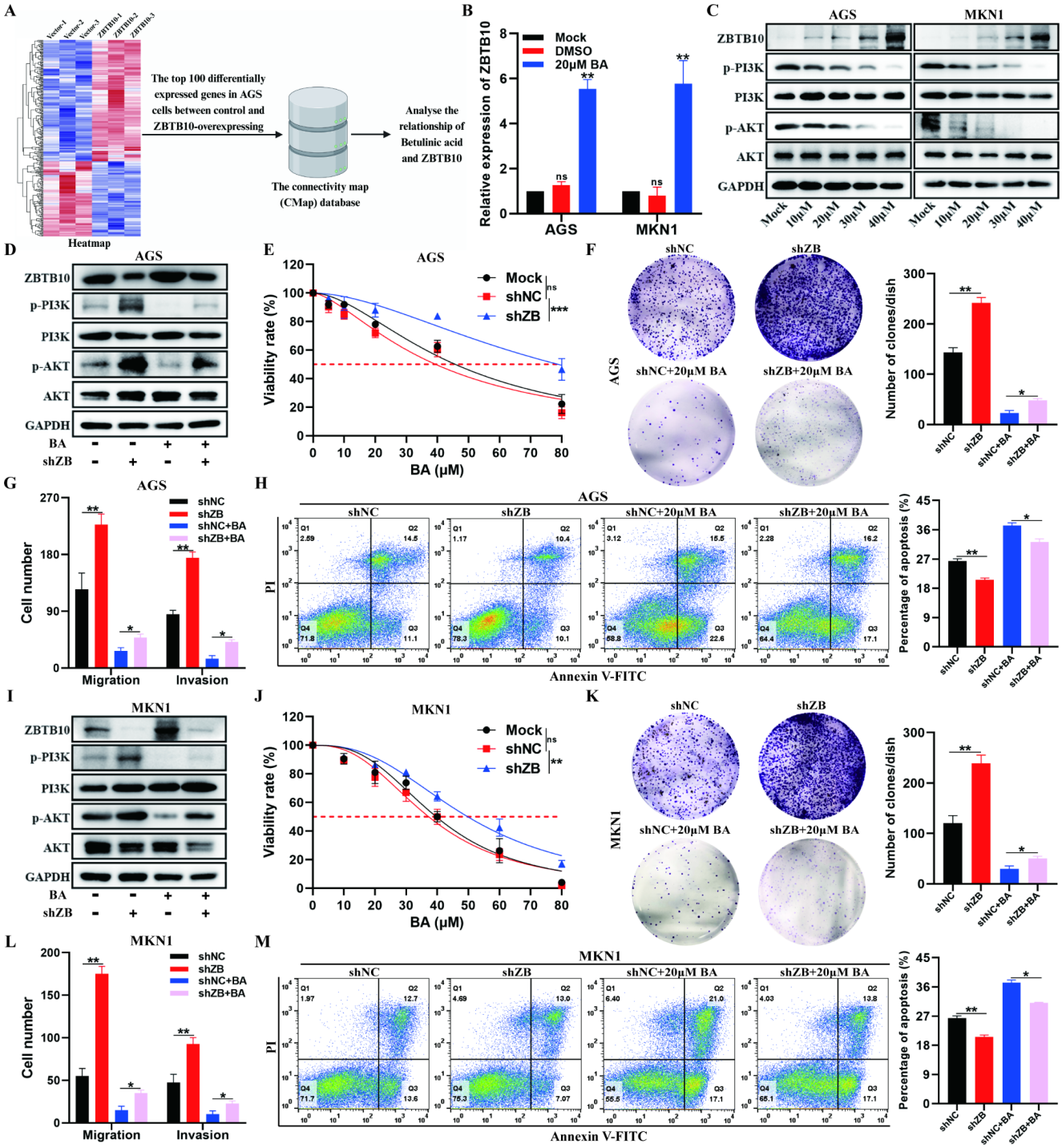

Fig. 6 ZBTB10 is a pivotal target for BA in inhibiting GC progression. **A** The mode diagram of analyzing the relationship between BA and ZBTB10 in cancer through CMAP database. **B** BA promoted ZBTB10 mRNA expression of AGS and MKN1 cells. **C** BA promoted ZBTB10 protein expression and inhibited p-PI3K and p-AKT protein expression with a concentration-dependent manner in AGS and MKN1 cells. **D**, **I** p-PI3K and p-AKT protein levels were increased following ZBTB10 knockdown and were rescued by BA (20μM) treatment. **E**, **J** The results of cell viability assay indicated that ZBTB10 knockdown in AGS (E) and MKN1 (J) cells would increase their resistance to BA. **F**, **K** Representative images and quantitative results of colony formation assay of negative control or ZBTB10 knockdown AGS (F) and MKN1 (K) cells treated with DMSO or BA. **G**, **L** The migration and invasion ability of AGS (G) and MKN1 (L) cells was enhanced when ZBTB10 knockdown, and this effect was rescued after BA treatment. **H**, **M** Representative images and quantitative results of flow cytometric cell apoptosis analysis of negative control or ZBTB10 knockdown AGS (H) and MKN1 (M) cells treated with DMSO or BA. Data are expressed as mean ± SD of biological replicate experiments. $*p<0.05$, $**p<0.01$, $***p<0.001$

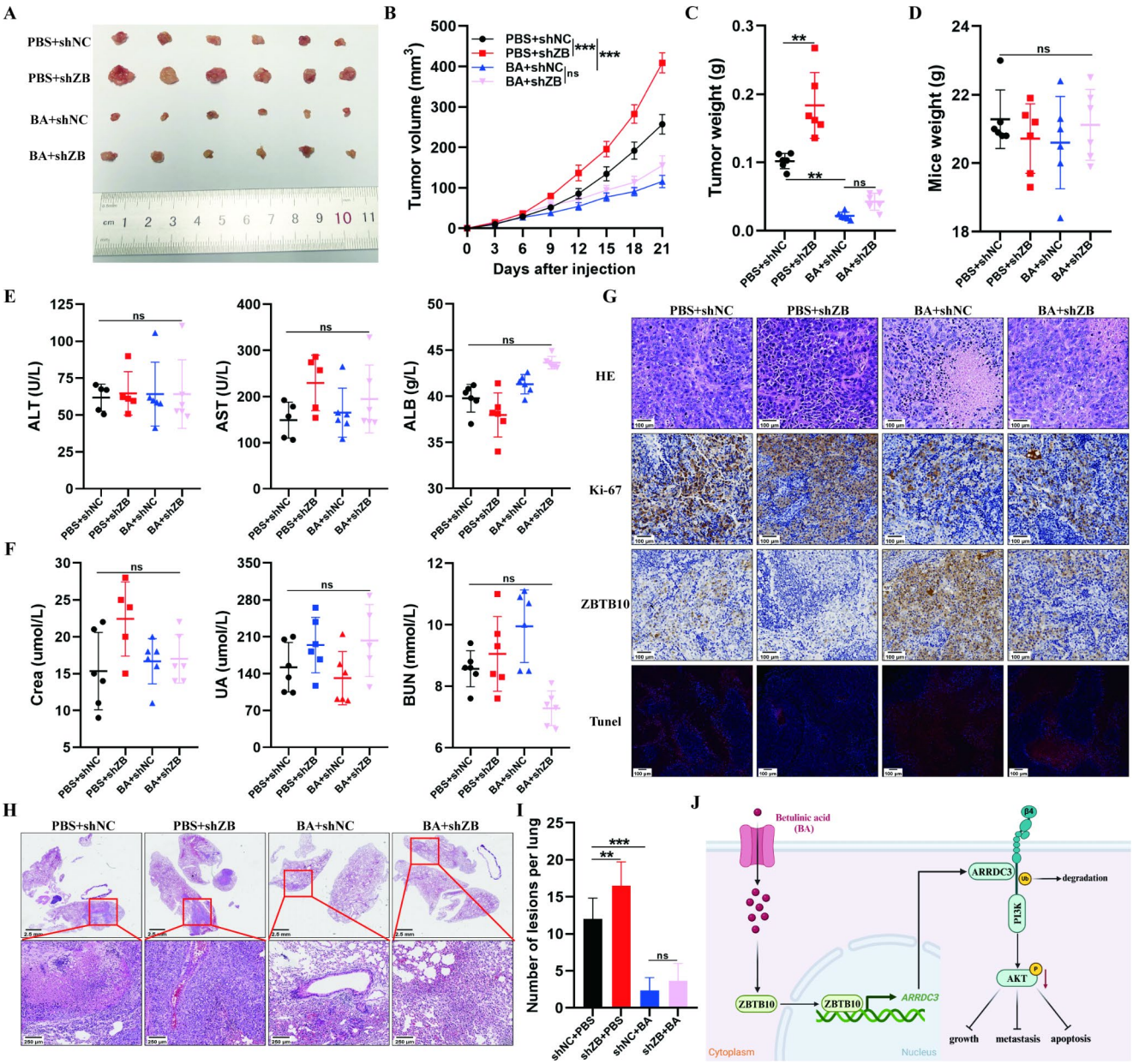

Fig. 7 BA inhibits GC tumorigenicity and metastasis by promoting ZBTB10 expression in vivo. **A-C** Image of xenograft tumor samples (A), tumor volumes (B), and tumor weights (C) derived from mice injected with ZBTB10 knockdown or negative control MGC803 cells and treated with BA or PBS. scale bar: 200 μm. **D-F** Body weight (D), liver function (E) and renal function (F) of the mice in each group. **G** Representative images of HE staining and IHC staining for ZBTB10, Ki-67, and TUNEL ($n=6$). **H** Representative HE staining images of lung samples from the indicated groups. Scale bars: 2.5 mm (upper panel) and 250 μm (lower panel). **I** Quantitative results of the metastatic nodes of the lungs in Fig. 7H. **J** Illustrative model showing the proposed mechanism by which enhanced ZBTB10 expression induced by betulinic acid inhibits gastric cancer progression by inactivating the ARRDC3/ITGB4/PI3K/AKT pathway. *$p<0.05$, **$p<0.01$, ***$p<0.001$

the progression of prostate cancer through ARRDC3/ITGB4 pathway [26]. Given that integrins, including ITGB4, are known regulators of the PI3K/AKT pathway [27], and that ARRDC3 has been shown to inhibit liver fibrosis and epithelial-to-mesenchymal transition via the ITGB4/PI3K/AKT pathway [24], we hypothesized that ZBTB10 inactivates the PI3K/AKT pathway through the ARRDC3/ITGB4 axis. Further investigation revealed that ARRDC3 downregulation in GC tissues was correlated with poor prognosis and that ARRDC3 inhibited GC cell proliferation and metastasis *in vitro*. Moreover, we demonstrated that ZBTB10 transcriptionally activated ARRDC3, which then directly bound to ITGB4, leading to its ubiquitination and degradation. This process ultimately reduced the phosphorylation levels

of PI3K and AKT. In all, ARRDC3 is indispensable for the inhibition of PI3K/AKT pathway and GC progression regulated by ZBTB10, elucidating the role of the ZBTB10/ARRDC3/ITGB4 axis in this context.

Currently, the prognosis for the patients with advanced GC remains poor due to high recurrence rates, metastasis, and the lack of effective treatments [42]. The search for novel, safe, and effective therapeutic agents is ongoing. Recent studies have highlighted the potential of small natural compounds as effective anti-tumor agents [43]. ZBTB10 has also been identified as a target for several anti-cancer drugs [29, 30], prompting us to investigate its potential as a target for anti-GC drugs using the CMap database. The results suggested that ZBTB10 might be a key target for BA in inhibiting GC progression. BA, a natural pentacyclic terpene, has demonstrated anti-cancer activity against various malignancies, including GC [18–20]. Moreover, derivatives of BA have been used for the clinical treatment of numerous cancers [44, 45]. Notably, BA has also been reported to play a role by promoting ZBTB10 expression in other cancers [16, 46]. However, this has not been reported in GC. Furthermore, the effect of BA on GC and its biosafety in vivo have not been reported. Our study revealed, for the first time, that BA inhibited GC tumorigenicity and metastasis in vivo and was safe in mice, providing strong evidence for its potential clinical use. In addition, we also demonstrated that ZBTB10 was one of the targets for BA in inhibiting GC progression. Combined with all of the above data, we believe that ZBTB10 is a novel therapeutic target and BA might act as feasible therapeutic strategy for GC.

5 Conclusions

Our study reveals that that ZBTB10 and BA inhibit GC progression both in vitro and *in vivo*. BA-induced upregulation of ZBTB10 transcriptionally activates ARRDC3, which then binds to ITGB4, leading to its ubiquitination and degradation. This results in the downregulation of PI3K and AKT phosphorylation level. Thus, BA could be a valuable treatment for GC, and the ZBTB10/ARRDC3/ITGB4/PI3K/AKT axis may serve as a novel diagnostic and therapeutic target. Nevertheless, due to the limitations of this study, there are important aspects that are not fully discussed. First, the molecular mechanism on BA regulating ZBTB10 expression remains unclear and will be explored in our subsequent studies. Second, we do not investigate the relationship between ZBTB10 and tumor microenvironment and drug resistance of GC cells, and the efficacy of BA combined with chemotherapy and immunotherapy.

Supplementary Information The online version contains supplementary material available at https://doi.org/10.1007/s13402-025-01039-8 .

Author contributions Zhixin Huang: Writing – original draft, Investigation, Methodology, Formal analysis, Data curation, Conceptualization. Ying Li: Writing – original draft, Writing – review & editing, Data curation. Zeyu Zhao: Writing – review & editing, Formal analysis, Data curation. Linying Ye: Methodology, Formal analysis. Tianhao Zhang: Methodology, Formal analysis, Funding acquisition. Zihan Yu: Methodology, Formal analysis. Ertao Zhai: Investigation, Data curation. Yan Qian: Formal analysis, Software, Funding acquisition. Xiang Xu: Methodology, Formal analysis. Risheng Zhao: Methodology, Data curation, Funding acquisition. Shirong Cai: Validation, Supervision, Resources, Project administration, Funding acquisition. Jianhui Chen: Validation, Supervision, Resources, Project administration, Funding acquisition.

Funding This work was supported by the National Natural Science Foundation of China (grant numbers: 82173239, 82100626, and 82472904); the Natural Science Foundation of Guangdong Province (grant numbers: 2022A1515011534, 2023A1515011187, and 2024A1515010739); the 5010 project of the First Affiliated Hospital of Sun Yat-sen University (grant number: 2018004); the Guangzhou Basic and Applied Basic Research Foundation (grant number: 202201010777, and 2024A04J4699); the Guangdong Province Regional Joint Fund—Youth project (grant number: 2023A1515111152); the Young Teacher Training Project of Sun Yat-sen University (grant number: 24qnpy329), and the GDAS' Special Project of Science and Technology Development (grant number: 2021GDASYL-20210103012).

Data availability No datasets were generated or analysed during the current study.

Declarations

Ethical approval This study was approved by the Institutional Ethical Boards of the First Affiliated Hospital of Sun Yat-sen University. Written informed consent was obtained from all patients. The animal study was carried out in compliance with the guidance suggestion of Animal Care Committee of the First Affiliated Hospital of Sun Yat-sen University.

Competing interests The authors declare no competing interests.

References

1. E.C. Smyth, M. Nilsson, H.I. Grabsch, van N.C. Grieken, F. Lordick, Gastric cancer. Lancet. **396**, 635–648 (2020)
2. H. Qiu, S. Cao, R. Xu, Cancer incidence, mortality, and burden in China: a time-trend analysis and comparison with the United States and United Kingdom based on the global epidemiological data released in 2020. Cancer Commun. (Lond). **41**, 1037–1048 (2021)
3. H. Sung, J. Ferlay, R.L. Siegel, M. Laversanne, I. Soerjomataram, A. Jemal et al., Global Cancer statistics 2020: GLOBOCAN estimates of incidence and Mortality Worldwide for 36 cancers in 185 countries. CA Cancer J. Clin. **71**, 209–249 (2021)
4. W.-L. Guan, Y. He, R.-H. Xu, Gastric cancer treatment: recent progress and future perspectives. J. Hematol. Oncol. **16**, 57 (2023)
5. S.-U. Lee, T. Maeda, POK/ZBTB proteins: an emerging family of proteins that regulate lymphoid development and function. Immunol. Rev. **247**, 107–119 (2012)
6. W. Xu, H. Yao, Z. Wu, X. Yan, Z. Jiao, Y. Liu et al., Oncoprotein SET-associated transcription factor ZBTB11 triggers lung cancer metastasis. Nat. Commun. **15**, 1362 (2024)
7. S.U. Mertens-Talcott, S. Chintharlapalli, X. Li, S. Safe, The oncogenic microRNA-27a targets genes that regulate specificity protein transcription factors and the G2-M checkpoint in MDA-MB-231 breast cancer cells. Cancer Res. **67**, 11001–11011 (2007)
8. W. Tang, F. Yu, H. Yao, X. Cui, Y. Jiao, L. Lin et al., miR-27a regulates endothelial differentiation of breast cancer stem like cells. Oncogene. **33**, 2629–2638 (2014)
9. A. Bluhm, N. Viceconte, F. Li, G. Rane, S. Ritz, S. Wang et al., ZBTB10 binds the telomeric variant repeat TTGGGG and interacts with TRF2. Nucleic Acids Res. **47**, 1896–1907 (2019)
10. S. Smita, A. Ghosh, V.K. Biswas, A. Ahad, S. Podder, A. Jha et al., Zbtb10 transcription factor is crucial for murine cDC1 activation and cytokine secretion. Eur. J. Immunol. **51**, 1126–1142 (2021)
11. Y.-C. Wen, W.-Y. Chen, V.T.N. Tram, H.-L. Yeh, W.-H. Chen, K.-C. Jiang et al., Pyruvate kinase L/R links metabolism dysfunction to neuroendocrine differentiation of prostate cancer by ZBTB10 deficiency. Cell. Death Dis. **13**, 252 (2022)
12. Q. Sun, H. Gu, Y. Zeng, Y. Xia, Y. Wang, Y. Jing et al., Hsa-mir-27a genetic variant contributes to gastric cancer susceptibility through affecting miR-27a and target gene expression. Cancer Sci. **101**, 2241–2247 (2010)
13. Y. Tan, R. Yu, J.M. Pezzuto, Betulinic acid-induced programmed cell death in human melanoma cells involves mitogen-activated protein kinase activation. Clin. Cancer Res. **9**, 2866–2875 (2003)
14. S. Alakurtti, T. Mäkelä, S. Koskimies, J. Yli-Kauhaluoma, Pharmacological properties of the ubiquitous natural product betulin. Eur. J. Pharm. Sci. **29**, 1–13 (2006)
15. H. Kasperczyk, La K. Ferla-Brühl, M.A. Westhoff, L. Behrend, R.M. Zwacka, K.-M. Debatin et al., Betulinic acid as new activator of NF-kappaB: molecular mechanisms and implications for cancer therapy. Oncogene. **24**, 6945–6956 (2005)
16. X. Liu, I. Jutooru, P. Lei, K. Kim, S. Lee, L.K. Brents et al., Betulinic acid targets YY1 and ErbB2 through cannabinoid receptor-dependent disruption of MicroRNA-27a:ZBTB10 in breast Cancer. Mol. Cancer Ther. **11**, 1421–1431 (2012)
17. Y. Cai, Y. Zheng, J. Gu, S. Wang, N. Wang, B. Yang et al., Betulinic acid chemosensitizes breast cancer by triggering ER stress-mediated apoptosis by directly targeting GRP78. Cell. Death Dis. **9**, 636 (2018)
18. X. Chen, X. Yuan, Z. Zhang, P. Gong, W. Yin, Q. Jiang et al., Betulinic acid inhibits cell proliferation and migration in gastric cancer by targeting the NF-κB/VASP pathway. Eur. J. Pharmacol. **889**, 173493 (2020)
19. S.Y. Kim, H. Hwangbo, M.Y. Kim, S.Y. Ji, D.H. Kim, H. Lee et al., Betulinic Acid restricts human bladder Cancer Cell Proliferation in Vitro by inducing caspase-dependent cell death and cell cycle arrest, and decreasing metastatic potential. Molecules. **26**, 1381 (2021)
20. Y. Zhang, N. He, X. Zhou, F. Wang, H. Cai, S.H. Huang et al., Betulinic acid induces autophagy-dependent apoptosis via Bmi-1/ROS/AMPK-mTOR-ULK1 axis in human bladder cancer cells. Aging. **13**, 21251–21267 (2021)
21. Y. Liu, E. Zhai, J. Chen, Y. Qian, R. Zhao, Y. Ma et al., m6A-mediated regulation of PBX1-GCH1 axis promotes gastric cancer proliferation and metastasis by elevating tetrahydrobiopterin levels. Cancer Commun. (Lond). **42**, 327–344 (2022)
22. W. Wang, Y. Wang, M. Liu, Y. Zhang, T. Yang, D. Li et al., Betulinic acid induces apoptosis and suppresses metastasis in hepatocellular carcinoma cell lines in vitro and in vivo. J. Cell. Mol. Med. **23**, 586–595 (2019)
23. X. Shu, P.-P. Zhan, L.-X. Sun, L. Yu, J. Liu, L.-C. Sun et al., BCAT1 activates PI3K/AKT/mTOR pathway and contributes to the angiogenesis and tumorigenicity of gastric Cancer. Front. Cell. Dev. Biol. **9**, 659260 (2021)
24. B. Zhang, F. Wu, P. Li, H. Li, ARRDC3 inhibits liver fibrosis and epithelial-to-mesenchymal transition via the ITGB4/PI3K/Akt signaling pathway. Immunopharmacol. Immunotoxicol. **45**, 160–171 (2023)
25. K.M. Draheim, H.-B. Chen, Q. Tao, N. Moore, M. Roche, S. Lyle, ARRDC3 suppresses breast cancer progression by negatively regulating integrin beta4. Oncogene. **29**, 5032–5047 (2010)
26. Y. Zheng, Z.-Y. Lin, J.-J. Xie, F.-N. Jiang, C.-J. Chen, J.-X. Li et al., ARRDC3 inhibits the progression of human prostate Cancer through ARRDC3-ITGβ4 pathway. Curr. Mol. Med. **17**, 221–229 (2017)
27. M. Li, Y. Wang, M. Li, X. Wu, S. Setrerrahmane, H. Xu, Integrins as attractive targets for cancer therapeutics. Acta Pharm. Sin B **11**, 2726–2737 (2021)
28. J.F. Nabhan, H. Pan, Q. Lu, Arrestin domain-containing protein 3 recruits the NEDD4 E3 ligase to mediate ubiquitination of the beta2-adrenergic receptor. EMBO Rep. **11**, 605–611 (2010)
29. S. Sreevalsan, S. Safe, The cannabinoid WIN 55,212-2 decreases specificity protein transcription factors and the oncogenic cap protein eIF4E in colon cancer cells. Mol. Cancer Ther. **12**, 2483–2493 (2013)
30. E. Hedrick, X. Li, S. Safe, Penfluridol represses integrin expression in breast Cancer through induction of reactive oxygen species and downregulation of sp transcription factors. Mol. Cancer Ther. **16**, 205–216 (2017)
31. J. Lamb, E.D. Crawford, D. Peck, J.W. Modell, I.C. Blat, M.J. Wrobel et al., The Connectivity Map: using gene-expression signatures to connect small molecules, genes, and disease. Science. **313**, 1929–1935 (2006)
32. F.-H. Wang, X.-T. Zhang, L. Tang, Q. Wu, M.-Y. Cai, Y.-F. Li et al., The Chinese Society of Clinical Oncology (CSCO): clinical guidelines for the diagnosis and treatment of gastric cancer, 2023. Cancer Commun. (Lond). **44**, 127–172 (2024)
33. J.H. Laity, B.M. Lee, P.E. Wright, Zinc finger proteins: new insights into structural and functional diversity. Curr. Opin. Struct. Biol. **11**, 39–46 (2001)
34. A. Noman, M. Aqeel, N. Khalid, W. Islam, T. Sanaullah, M. Anwar et al., Zinc finger protein transcription factors: Integrated line of action for plant antimicrobial activity. Microb. Pathog. **132**, 141–149 (2019)
35. J. Jen, Y.-C. Wang, Zinc finger proteins in cancer progression. J. Biomed. Sci. **23**, 53 (2016)

36. S.U. Mertens-Talcott, G.D. Noratto, X. Li, G. Angel-Morales, M.C. Bertoldi, S. Safe, Betulinic acid decreases ER-negative breast cancer cell growth in vitro and in vivo: role of sp transcription factors and microRNA-27a:ZBTB10. Mol. Carcinog. **52**, 591–602 (2013)
37. A.S. Alzahrani, PI3K/Akt/mTOR inhibitors in cancer: at the bench and bedside. Semin Cancer Biol. **59**, 125–132 (2019)
38. L. Yu, J. Wei, P. Liu, Attacking the PI3K/Akt/mTOR signaling pathway for targeted therapeutic treatment in human cancer. Semin Cancer Biol. **85**, 69–94 (2022)
39. S. Wu, M. Chen, J. Huang, F. Zhang, Z. Lv, Y. Jia et al., ORAI2 promotes gastric Cancer Tumorigenicity and Metastasis through PI3K/Akt signaling and MAPK-Dependent focal adhesion disassembly. Cancer Res. **81**, 986–1000 (2021)
40. H.-T. Liu, Y.-X. Zou, W.-J. Zhu, G.-H. Sen-Liu null, Zhang, R.-R. Ma et al., lncRNA THAP7-AS1, transcriptionally activated by SP1 and post-transcriptionally stabilized by METTL3-mediated m6A modification, exerts oncogenic properties by improving CUL4B entry into the nucleus. Cell. Death Differ. **29**, 627–641 (2022)
41. H. Wedegaertner, W.-A. Pan, C.C. Gonzalez, D.J. Gonzalez, J. Trejo, The α-Arrestin ARRDC3 is an emerging multifunctional adaptor protein in Cancer. Antioxid. Redox Signal. **36**, 1066–1079 (2022)
42. S.S. Joshi, B.D. Badgwell, Current treatment and recent progress in gastric cancer. CA Cancer J. Clin. **71**, 264–279 (2021)
43. Z. Ma, X. Xiang, S. Li, P. Xie, Q. Gong, B.-C. Goh et al., Targeting hypoxia-inducible factor-1, for cancer treatment: recent advances in developing small-molecule inhibitors from natural compounds. Semin Cancer Biol. **80**, 379–390 (2022)
44. P. Gonzalez, I. Mader, A. Tchoghandjian, S. Enzenmüller, S. Cristofanon, F. Basit et al., Impairment of lysosomal integrity by B10, a glycosylated derivative of betulinic acid, leads to lysosomal cell death and converts autophagy into a detrimental process. Cell. Death Differ. **19**, 1337–1346 (2012)
45. Y. Zhang, S. Ye, Y. Wang, C. Wang, Y. Zhu, Y. Wu et al., Discovery and optimization of betulinic acid derivatives as novel potent CD73 inhibitors. Bioorg. Med. Chem. **59**, 116672 (2022)
46. S. Chintharlapalli, S. Papineni, P. Lei, S. Pathi, S. Safe, Betulinic acid inhibits colon cancer cell and tumor growth and induces proteasome-dependent and -independent downregulation of specificity proteins (sp) transcription factors. BMC Cancer. **11**, 371 (2011)